Energy and Buildings 126 (2016) 14–27

Contents lists available at ScienceDirect

Energy and Buildings

journal homepage: www.elsevier.com/locate/enbuild

Numerical analysis on the cooling performance of a ventilated Trombe wall combined with venetian blinds in an office building

Zhongting Hu [a], Wei He [b,*], Xiaoqiang Hong [a], Jie Ji [a], Zhihe Shen [b]

[a] Department of thermal Science and Energy Engineering, University of Science and Technology of China, Hefei 230026, China
[b] Department of Building Environment and Equipment, Hefei University of Technology, Hefei 230009 China

ARTICLE INFO

Article history:
Received 3 December 2015
Received in revised form 26 April 2016
Accepted 6 May 2016
Available online 10 May 2016

Keywords:
Numerical model
Trombe wall
Venetian blinds
Split-type air conditioner
Cooling load reduction
Office building

ABSTRACT

Using a Trombe wall with venetian blinds (VBTW) as a cooling system in an office building with split-type air conditioner and simultaneously considering the requirements of outdoor air supply are few investigated. A dynamic model on the VBTW was presented and validated by the experiment in this paper. The influence of three parameters in combination with two set-point temperatures 24 °C and 26 °C on the cooling load were investigated: blind tilt angles from the horizontal (15°, 45°, 60°, 75°), air gap width (5 cm, 10 cm, 15 cm and 20 cm), core layer materials (red brick 1760, red brick 1120, concrete block 1440 and concrete 2210) together with different thickness. The results indicated that by increasing the air gap width, the cooling load was increased a little. However, variations of the blind tilt angle have a significant effect on the cooling load. Bigger blind tilt angle (closing) yielded lower heat flux across the VBTW. Finally, the use of low instead of high density materials in the core may reduce the cooling load. The heat-transfer rate through the wall depended on the compared thermal conductivity and their thermal capacity. The afore-mentioned findings are helpful for the energy saving design of the solar utilization.

1. Introduction

Today's buildings are dominated by the 'active' environmental control system for heating, ventilation and air conditioning often resulting in an increase in conventional energy use and CO_2 emission. Therefore, we need to actively seek renewable energy technology to relieve building energy consumption [1]. Among the renewable sources, solar energy plays the most import role due to its infinity and cleanness. Trombe wall is a sustainable architectural technology of the solar energy utilization for space heating and ventilation [2,3]. A conventional Trombe wall is a system that makes use of indirect solar gain [4]. It is normally comprised of a massive wall painted black, an exterior glazing cover and a ventilated air gap in between [5]. Two adjustable dampers at the massive wall and adjustable vent of the glazing cover are designed for winter heating and summer cooling. The blackened massive wall absorbs and stores the solar energy transmitted through the glazing. Heat exchange of Trombe wall with the indoor environment is partly by conduction through the wall and partly by ventilation through the vents due to buoyancy effect [6].

The Trombe wall is mainly used in cold and mild climates for passive solar heating. It can reduce a building's energy consumption for residential heating by up to 30% [7]. There have been numerous studies on the Trombe wall for passive solar heating: Khalifa and Abbas et al. [8] numerically study the effect of storage wall material and thickness on room temperature. Similar studies are conducted by [9–11]. In this direction, Agrawal and Tiwari have proposed an optimal thickness of 30–40 cm for a concrete Trombe wall [12]. Chen et al. [13] conducted an experiment of Trombe wall with shading device and found that the use of shading can reduce about 20%–40% heat loss in the air gap on a winter night. Several studies on the Trombe wall for passive cooling focused on reducing the drawback of the Trombe wall in summer for hot climates: Ghrab-Morcos et al. [14] described that overhangs in Trombe wall were of valuable aid to against overheating. Ji et al. [15] proposed that appending a shading curtain in summer were adopted for PV-Trombe wall. Similarly, Soussi et al. [16] pointed out that the building with properly shielded Trombe wall can reduce the annual cooling requirements. Gan et al. [17,18] carried out the numerical simulation of a Trombe wall for summer cooling and investigated the effect of the wall height and insulation. Stazi et al. [19] adopted some strategies to enhance the efficiency of Trombe walls in summer time. Rabani et al. [20,21] presented an experimental study of a new designed Trombe wall in combination with solar chimney and water spraying system. The results demonstrated that the new

* Corresponding author.
E-mail address: hwei@hfut.edu.cn (W. He).

http://dx.doi.org/10.1016/j.enbuild.2016.05.016
0378-7788/

Nomenclature

A	Area (m^2)
c	Specific heat capacity (J/(kg K))
d	Air gap hydraulic diameter (m)
D	Air gap width (m)
E	Daily cooling load (KJ/m^2)
F	View factor
g	Gravitational acceleration (m/s^2)
H	Height of the VBTW (m)
h	Heat transfer coefficient (W/m^2 K)
I	Vertical solar radiation ($W\ m^{-2}$)
m	Mass (kg)
Nu	Nusslet number
Pr	Prandtl number
P	Permeability
q	Heat flux across the wall (W/m^2)
Re	Reynolds number
si	Blind tilt angle (°)
T	temperature (°C)
t	Time (s)
V	Air velocity (m/s)
$\dot{V}_{bz}$	Ventilation rates (m^3/h)

Greek symbols

α	Absorptivity
β	Heat expansion coefficient (K^{-1})
λ	Thermal conductivity (W/(m °C)
ε	Emissivity
τ	Transmittance
ρ	Density (Kg/m^3)
ϕ	Absorbed solar energy (W)
η	Cooling load reduction

Subscripts

a	Air in the air duct
b	Venetian blinds
c	Convection heat transfer
f	Fan
g	Glazing cover
r	Radiation heat transfer
w	Trombe wall with venetian blinds
nw	Normal south wall
in	Air inlet
out	Air outlet

designed Trombe wall can decrease indoor temperature by about 8 °C in hot season.

In recent studies, a novel Trombe wall combined with venetian blinds (VBTW) was proposed by the present authors [22,23]. The amount of absorbed solar radiation can be controlled by adjusting the angle of venetian blinds to achieve a relatively stable and comfortable indoor condition. The present authors emphasized the winter performance of the VBTW and found that the VBTW was more effective when used in office buildings [23]. At hot summer and cold winter area in China, office buildings are normally equipped with split-type air conditioners. In summer, outdoor air supply to the office building is by fortuitous ventilation through cracks and openings in the building fabric. However, as a result of wide-spread draught proofing of doors, windows, etc., office buildings have become less well ventilated [24]. Therefore, well-designed natural or mechanical ventilation system are required to provide comfortable and healthy conditions for its occupants. Trombe wall with venetian blinds (VBTW) is treated as an ingenious design for addressing ventilation issues due to its simple geometry and non-additional air channel cost. Meanwhile, the loss of heat through ventilation can be used to cool building envelope. Therefore, the VBTW can reduce air conditioner energy consumption without sacrificing the indoor air quality. Few investigations have been reported on the summer performance of the VBTW when applied in an office building with air conditioner, which was still unclear up to now. The principal purpose of this paper was to investigate the cooling load reduction of the VBTW compared with the normal south wall. To this end, this study was structured in two parts. The first part outlined the model of the VBTW summer mode, and went on to describe the validation process using the experimental results. The second part of this paper presented a parametric study when using the VBTW on an office building of 20 m^2. It is noteworthy that some part of the model is too simplified to match the testing results well. Thus, the present paper only investigated the cooling load and few parameters effects and didn't refer to some issues, such as the VBTW's cost efficiency, the payback time, VBTW's maintenance and the effect of fan position.

2. Experimental setup

2.1. Description of the experimental platform

In our previous study [23], the experimental cells have been built in Hefei, China. Its average elevation is 26.8 m, latitude 31°52′N, and longitude 117 17′E. Hefei enjoys the subtropical humid monsoon climate with four distinct seasons (winter, spring, summer, and autumn). The climate is characterized by relatively hot summer and cold winter. The cooling days are between June and September.

The experiment cells consist of two rooms (right: test room, left: reference room) with interior dimensions of width 3800 mm/depth 3900 mm/height 2600 mm (see Fig. 1). Each room has been installed a split-type air conditioner and is oriented due south. All the building envelopes are insulated except the south wall. The two ventilated VBTWs have been applied on the south wall of the test room to maximize capture of sun rays, as shown in Fig. 2. To validate the summer model of the VBTW, we conducted the experiments on the afore-mentioned test room (left room in Fig. 1). The whole south wall comprises the VBTW part and the normal south wall part (see Figs. 1 and 2). In addition, the glazing and the outer surface of normal south wall are in a same plane. The ventilated VBTW, as shown in Fig. 3, was composed of a glazing cover, a massive wall behind venetian blinds, and a ventilated air gap in between. The proposed venetian blinds were characterized by selective absorption: one side of venetian blinds was covered with high absorptivity coating (blue titanium, 0. 9) and the other side was covered high reflectivity coating (aluminum film, 0.15). The side with high absorptivity coating is overturned outward in winter. In contrary, in hot season the other side with high reflectivity coating face the sun to prevent overheating effect. The venetian blinds can be placed in the out surface of the glazing or in the air gap. However, locating the venetian blinds in air gap can prolong its using life and improve the aesthetic appealing look of the system. Moreover, the buoyancy effect can be enhanced to reduce the energy consumption of the fan. Therefore, in our study the venetian blinds was installed in the air gap. In addition, the outer glazing can be opened for the maintenance of the system. There are two air vents for winter heating and two air vents for summer cooling. For summer cooling, the lower vent at the massive wall and the vent at the glazing cover are opened. The solar heated air in the air gap draws room air from the lower vent at the massive wall and the heated air is then flows out to the ambient through the vent at the glazing cover. The driving force which controls the airflow rate is generated by the buoyancy effect and a fan. The normal south wall as well as massive wall has three layers:

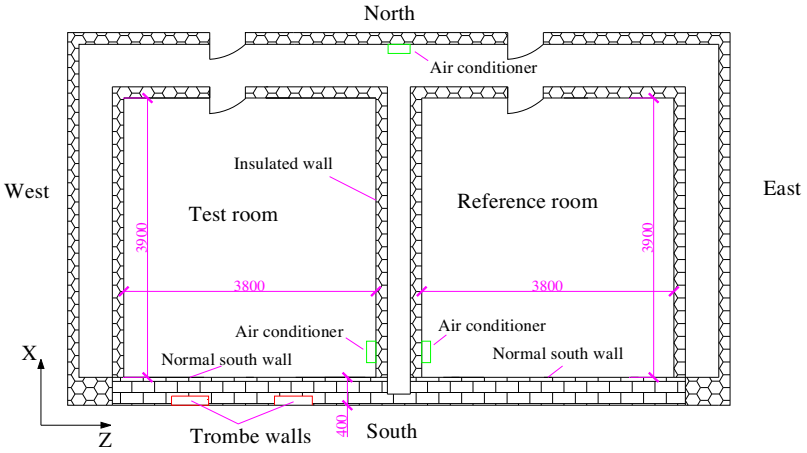

Fig. 1. The horizontal cross-section schematic of the experimental platform.

Fig. 2. South façade view of the test room (left) and the reference room (right).

outer lime layer, core layer (red brick 1760), and inner lime layer. Fig. 4 showed the structure of normal south wall (left) and massive wall (right). Detail characteristics of the VBTW were as follows:

(1) Azimuth surface angle of the VBTW, $az_w = 0$ (South orientation).
(2) Massive wall height, H = 2 m.
(3) Massive wall width, L = 1m.
(4) Massive wall thickness, $D_w = 24$ cm.
(5) Air gap width, Da = 16 cm.
(6) Red brick conductivity, $\lambda_w = 0.814$ (W/m K^{-1}).
(7) Specific heat and density of the red brick, $C_w = 840$ (J/kg K^{-1}), $\rho_w = 1760$ (kg/m^3).
(8) Solar absorption of the massive wall, $\alpha_w = 0.9$.
(9) Emissivity of the massive wall, $\varepsilon_w = 0.9$.
(10) Venetian blind width and length, sw = 2.5 cm, $L_b = 0.9$ m.
(11) Specific heat of the blinds, $C_b = 875$ (J/kg K^{-1}), and density $\rho_b = 2750$ (kg/m^3).
(12) Absorptivity of venetian blinds with high reflectivity, $\alpha_{b1} = 0.15$.
(13) Absorptivity of venetian blinds with high absorptivity, $\alpha_{b2} = 0.9$.
(14) Distance between the blinds and massive wall, D = 8 cm.
(15) Glazing absorptivity, $\alpha_g = 0.15$, and transmissivity, $\tau_g = 0.85$.
(16) Number of glazing, $N_g = 1$.
(17) Glass thickness, Dg = 5 mm.
(18) Each vent area, At = 0.4 × 0.1 = 0.04 m^2.

2.2. Experimental measuring procedure

The experiment was conducted from August 1th to August 31th 2013. During the whole test procedure, only the left room in Fig. 1 (test room) was tested experimentally and the room air temperature was maintained at 26 °C by the air conditioner. The test time was from 08:00 to 16:00, i.e. the lower vent at the massive wall and the vent at the glazing cover were opened during the time

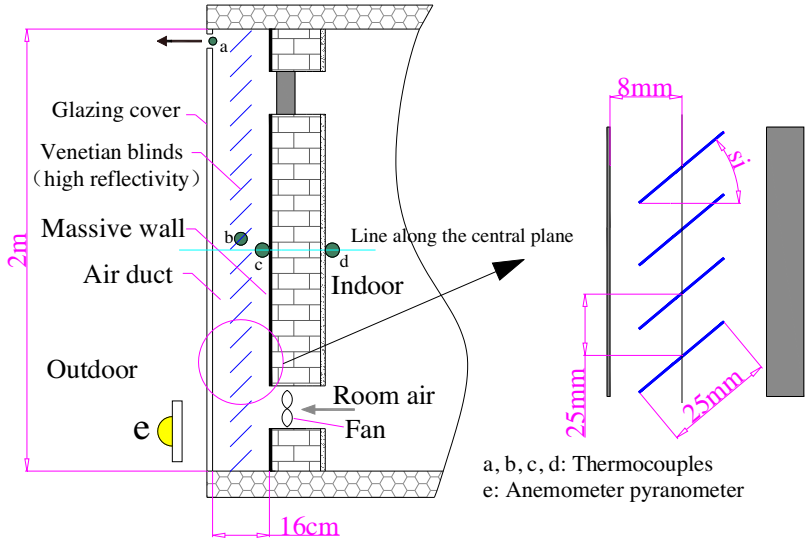

Fig. 3. VBTW system assisted with a fan for summer cooling and layout of testing points.

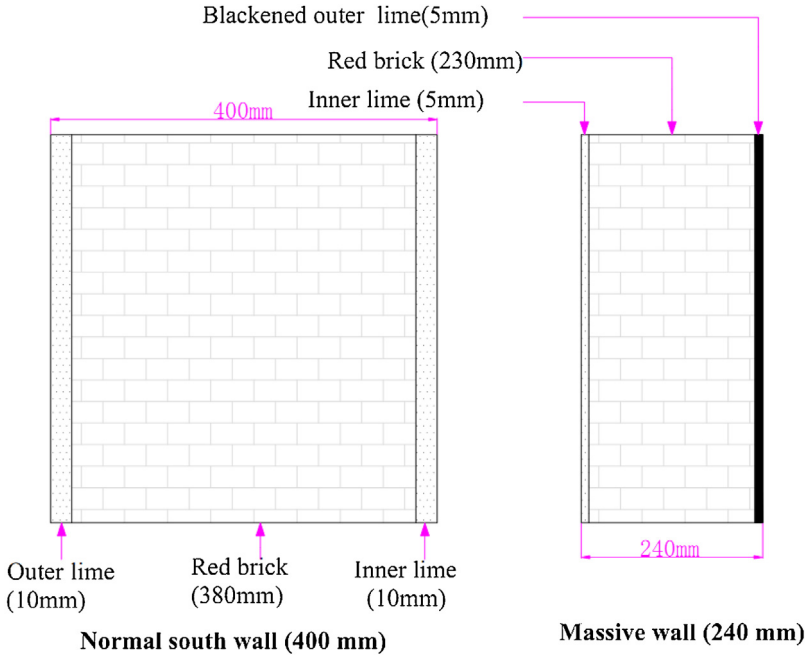

Fig. 4. Layers of the normal south wall and massive wall.

ranges. The venetian blinds were inclined at 80° from the horizontal. Testing parameters included the temperature and global solar radiation, which were measured by thermocouple thermometers (copper-constantan, ±0.5 °C) and solar pyranometer (TBQ-2, ±11.104 μv/W m^{-2} and ±11.601 μv/W m^{-2}), respectively. All of measured data were recorded every 30 s and saved in computer by a computerized data-logger. The test positions were shown in Fig. 3.

In addition, to enhance air flow from the room to the open atmosphere, the ventilation rates of the fan was controlled at 15 m^3/h.

3. Mathematical model

For the summer operation mode of the VBTW, the radiation transmission through blinds was divided into two different radiation paths: the unshaded transmission of the direct beam and the

Table 1
Comparisons between the simulated and experimental results.

Parameters	Root mean square error (RMSE)/°C	Mean absolute error (MAE)/°C
Outlet temperature	0.68	0.55
Venetian blinds	0.64	0.54
Internal surface temperature of massive wall	0.17	0.16
External surface temperature of massive wall	0.51	0.44

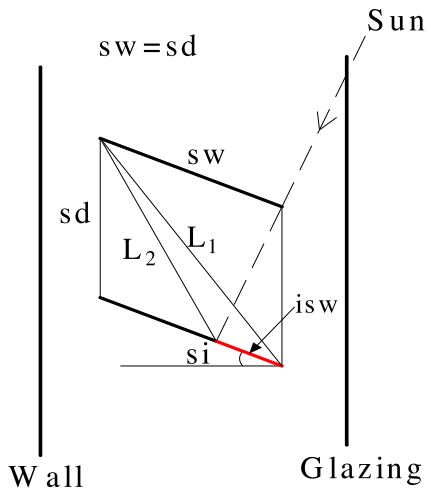

Fig. 5. Relationship between illuminated slat width, glazing and wall to illustrate the view factor f_1, f_2 and f_3.

direct-reflected beam from the illuminated slat surfaces. To prevent the light-pollution from the blinds, the side with high reflectivity coating for the venetian blinds was characterized by diffuse reflection. Therefore, the following assumption are established: The direct-reflected beam from the illuminated slat surfaces are pure diffuse. The detailed model of the VBTW has been given in our previous paper [23]. Therefore the only primarily equations and significant differences are given below for the VBTW system assisted with a fan.

3.1. Modeling of glazing

Since the glazing is very thin (5 mm), its temperature assumed uniform. In addition, the reflect effect from the glass is negligible.

$$m_g \times c_g \times \frac{dT_g}{dt} = A_g h_{conv-rad}(T_{eq} - T_g) + A_g h_{cg,a}(T_a - T_g) + A_g h_{rg,b}(T_b - T_g) + \phi_{sg} \quad (1)$$

$$\phi_{sg} = A_g \times (I \times \alpha_g + I_{si} \times \tau_g \times (1 - \alpha_{b1}) \times P_b \times f_1 \times \alpha_g) \quad (2)$$

where f_1 is the view factor between the illuminated slat area (*isw*) and the outer glass. The slat geometry is fully described by the slat width (sw) the slat distance (sd) and the slat inclination angle from the horizontal (si). The view factor f_1 can be calculated based on the cosine-law (see Fig. 5):

$$f_1 = \frac{isw + sd - \sqrt{sd^2 + isw^2 - 2 \times sd \times isw \times cos(90^\circ - si)}}{2 \times isw} \quad (3)$$

$$h_{cg,a} = \frac{Nu_d \times K_a}{d} \quad (4)$$

$$Nu_d = 0.023 Re^{4/5} Pr^{1/n} \quad (5)$$

where n = 0.3 when the fluid is cooling and n = 0.4 when the fluid is heated [25].

$$h_{rg,b} = \frac{4\sigma {T_m}^3}{(1/F_{g,b}) + (1 - \varepsilon_g)/\varepsilon_g + (1 - \varepsilon_{b1})/\varepsilon_{b1}} \quad (6)$$

$$F_{g,b} = 1 - \sin\left(\frac{90^\circ - s_i}{2}\right) \quad (7)$$

3.2. Modeling of air gap

Since the temperature stratification in the horizontal direction is not evident according to the Refs. [22,23], the air temperature in the air gap are only changed in the vertical direction.

$$\rho_a Dc_a \frac{dT_a}{dt} = h_{cg,a}(T_g - T_a) + h_{cw,a}(T_w - T_a) + h_{cb,a}(T_b - T_{ca}) - \rho_a V_a Dc_a \frac{dT_a}{dy} \quad (8)$$

$$V_a = \sqrt{\frac{g\beta(T_{out} - T_{in})H}{C_{in}(\frac{A}{A_{in}}) + C_{out}(\frac{A}{A_{out}}) + C_f(\frac{H}{d})}} + \frac{\dot{V}_f}{3600 A_{in}} \quad (9)$$

where $\dot{V}_f$ is the volume flow rate of the assisted fan, which can be given by the manufacturer; T_{in} is assumed to the room air temperature, which can be controlled by the air conditioner.

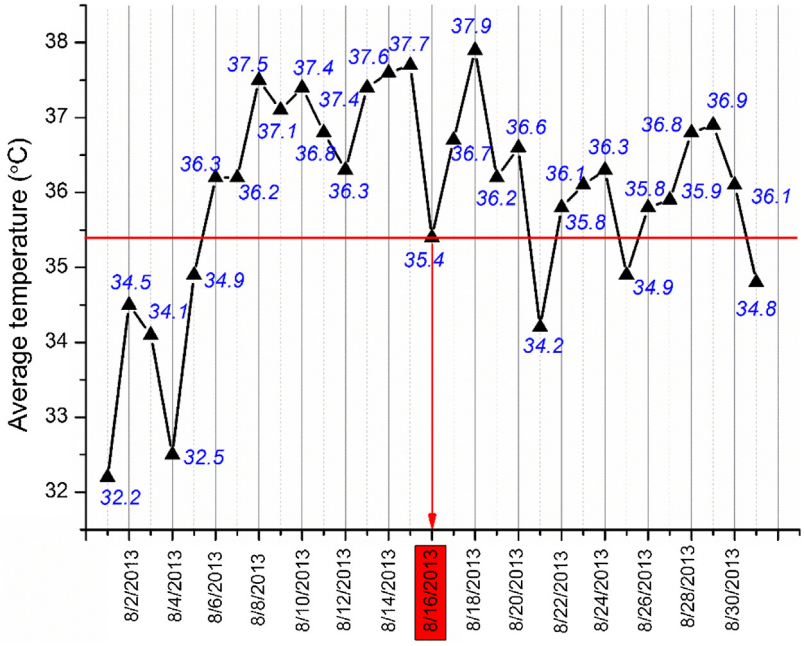

Fig. 6. Average daily outdoor temperature during August 2013.

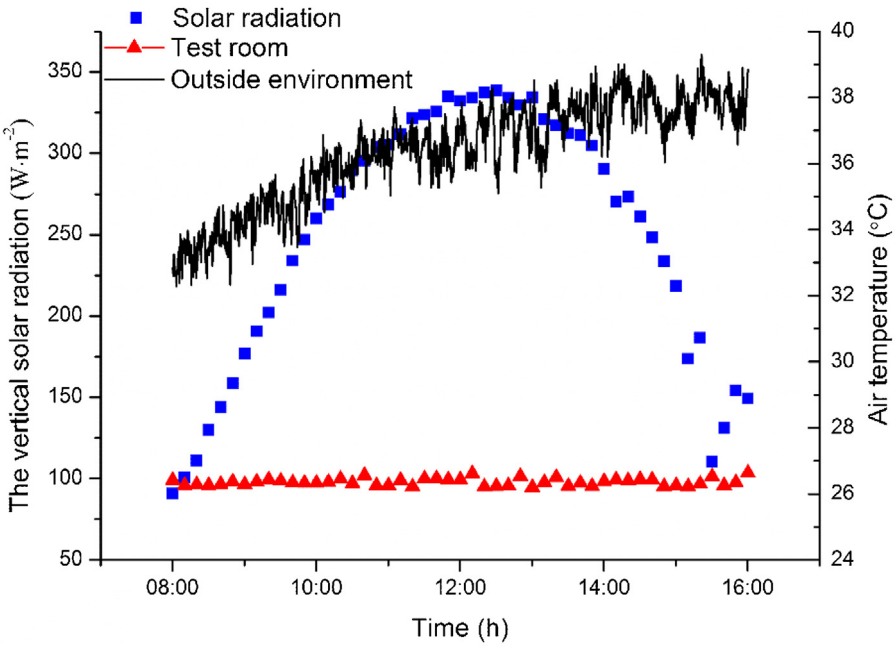

Fig. 7. Experimental data on August 16th, 2013.

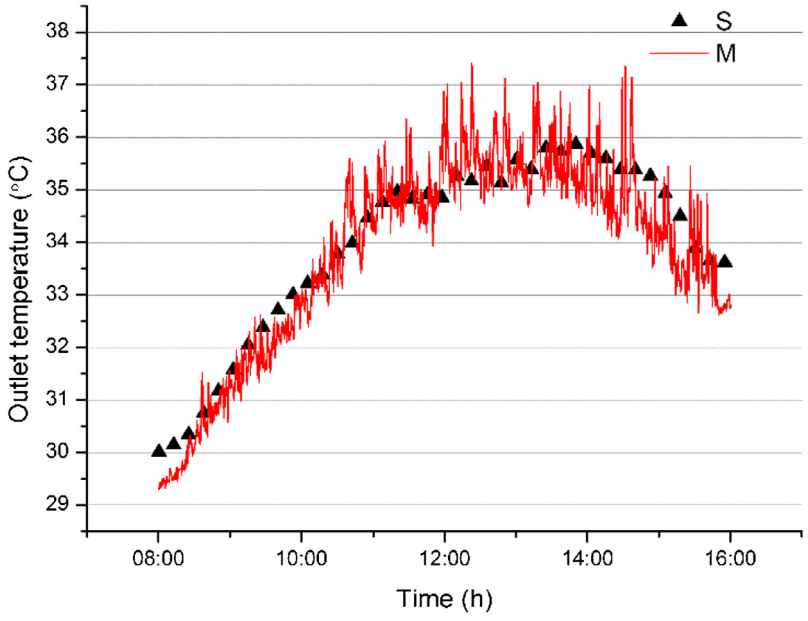

Fig. 8. Temperature of the outlet.

Table 2
Minimum ventilation rates for the office space.

Occupancy category	People Outdoor Air Rate R_p	Area Outdoor Air Rate R_a	Occupant Density	Zone population P_z	Ventilation rates $\dot{V}_{bz}$
	(L/s person)	(L/s m^2)	(Persons per 10 m^2)	(Persons)	(m^3/h)
Office space	2.5	0.3	1	2	40

3.3. Modeling of venetian blinds

The calculation considers temperature stratification in the vertical direction and the inter-reflections between the slats.

$$m_b c_b \frac{dT_b}{dt} = A_{L2} h_{cb,a}(T_a - T_b) + A_{L2} h_{rg,b}(T_g - T_b) + A_{L2} h_{rb,w}(T_w - T_b) + \phi_{sb1} + \phi_{sb2} \quad (10)$$

where ϕ_{sb1} is the direct sun flux absorbed by the illuminated slat surface, and ϕ_{sb1} is the direct-reflected solar flux absorbed by the slat under-surface. They can be expressed as:

$$\phi_{sb1} = \alpha_{b1} \tau_g I_{si} \times P_b \times A_b \quad (11)$$

$$\phi_{sb2} = f_3 \times (1 - \alpha_{b1}) \times \tau_g \times I_{si} \times P_b \times A_b \times \alpha_{b2} \quad (12)$$

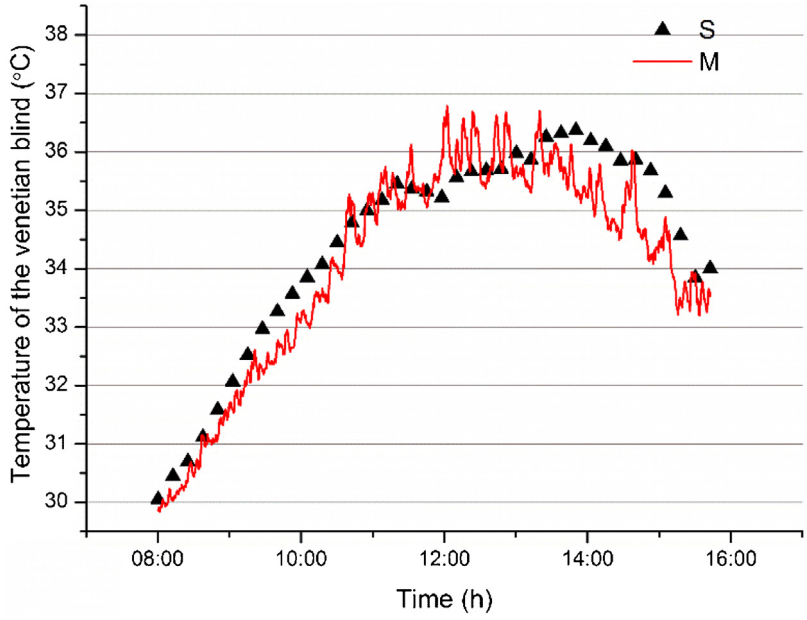

Fig. 9. Temperature of venetian blinds at mid-height of the VBTW.

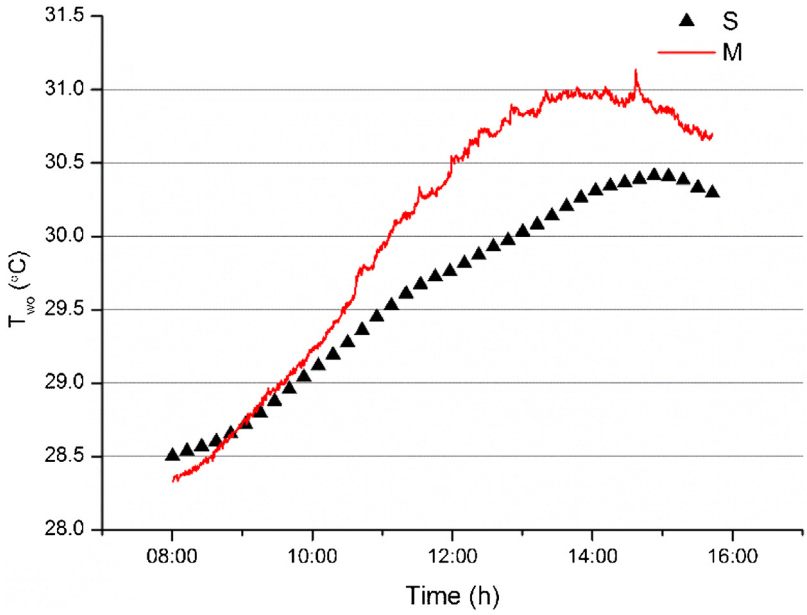

Fig. 10. Temperature of exterior surface of massive wall at mid-height of the VBTW.

where $f_2$is the view factor between the illuminated slat area (isw) and the upper slat, which can be calculated by:

$$f_2 = f_1 - f_3 \tag{13}$$

where f_1 and f_3 are given in Eqs. (3) and (20) respectively.

$$\begin{cases} P_b = 1 \\ P_w = 1 - (\sin(si) + \cos(si)\tan(h')) \end{cases} for P_b \geq 1 \tag{14}$$

$$\begin{cases} P_b = \dfrac{1}{\sin(si) + \cos(si)\tan(h')} \\ P_w = 0 \end{cases} for P_b < 1 \tag{15}$$

$$h' = \arctan\left(\frac{\sin(h_s)}{\cos(az_s\text{-}az_w)\cos(h_s)}\right) \tag{16}$$

3.4. Modeling of massive wall

The heat flux through the massive wall is determined by the one-dimensional along its thickness [26], and the energy balance equation is:

$$\frac{\partial T_w}{\partial t} = \frac{\lambda_w}{\rho_w c_w}\frac{\partial^2 T_w}{\partial^2 X} \tag{17}$$

$$-\lambda_w\left(\frac{\partial T_w}{\partial X}\right)_{x=0} = h_{cw,a} \times (T_w - T_a) + h_{rb,w}(T_w - T_b) + P_w \times \alpha_w \times \tau_g \times I + P_b \times I_{si} \times \tau_g \times (1 - \alpha_{b1}) \times f_2 \times \alpha_w \tag{18}$$

$$-\lambda_w\left(\frac{\partial T_w}{\partial X}\right)_{x=D_w} = h_{cw,r}(T_w - T_r) \tag{19}$$

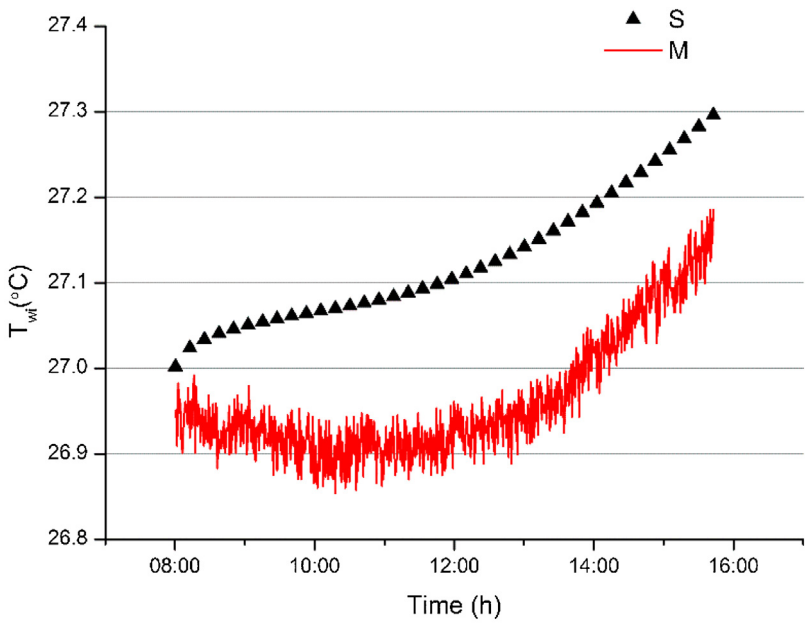

Fig. 11. Temperature of interior surface of massive wall at mid-height of the VBTW.

In Eq. (17), f_2 is the view factor between the illuminated slat area (isw) and the massive wall. According to Fig. 5, the view factor f_1 equals to the view factor slat area (isw) and L_1, which can be calculated by:

$$f_3 = \frac{isw + L_1 - L_2}{2 \times isw} \tag{20}$$

$$L_1 = sd \times \sqrt{2cos(90^\circ + si)} \tag{21}$$

$$L_2 = \sqrt{sd^2 + (sd - isw)^2 - 2sd \times (sd + isw) \times cos(90^\circ + si)} \tag{22}$$

3.5. Modeling of normal south wall

For the normal south wall (see Figs. 1 and 2), the absorbed solar radiation and heat conduction through the wall were considered, and the energy balance can be given as:

$$\frac{\partial T_{nw}}{\partial t} = \frac{\lambda_w}{\rho_w c_w} \frac{\partial^2 T_{nw}}{\partial^2 X} \tag{23}$$

$$-\lambda_w \left(\frac{\partial T_{nw}}{\partial X}\right)_{x=0} = h_{con-rad}(T_{nw} - T_{eq}) + \alpha_{nw} \times I_{90^\circ} \tag{24}$$

$$-\lambda_w \left(\frac{\partial T_{nw}}{\partial X}\right)_{x=D_{nw}} = h_{cw,r}(T_{nw} - T_r) \tag{25}$$

3.6. Energy performance

In order to evaluate the summer energy performance of the ventilated VBTW, the instantaneous value of the conductive heat flux across the massive wall (q_w) and normal south wall (q_{nw}) has been calculated, respectively.

$$q_w(t) = (T_{wi}(t) - T_{we}(t))/R_w \tag{26}$$

$$q_{nw}(t) = (T_{nwi}(t) - T_{nwe}(t))/R_{nw} \tag{27}$$

where R_w and R_{nw} are thermal resistance of normal south wall and massive wall respectively, and can be expressed as:

$$R_w = \frac{\lambda_{w1}}{D_{w1}} + \frac{2\lambda_{w2}}{D_{w2}} \tag{28}$$

$$R_{nw} = \frac{\lambda_{nw1}}{D_{nw1}} + \frac{2\lambda_{nw2}}{D_{nw2}} \tag{29}$$

The daily cooling load ($KJ \times m^{-2}$) for the two walls have been estimated as follows:

$$E_w = \int_{t_1}^{t_2} q_w(t')dt' = \frac{1}{R_w} \int_{t_1}^{t_2} (T_{we}(t') - T_{wi}(t'))dt' \tag{30}$$

$$E_{nw} = \int_{t_1}^{t_2} q_{nw}(t')dt' = \frac{1}{R_{nw}} \int_{t_1}^{t_2} (T_{nwe}(t') - T_{nwi}(t'))dt' \tag{31}$$

Therefore, the daily cooling load reduction of the VBTW compared to the normal south wall of the same size and materials can be calculated by:

$$\eta = \frac{E_{nw} - E_w}{E_{nw}} \times 100\% \tag{32}$$

4. Results and discussion

4.1. Model validation

Since the average outdoor temperature on 16th August was close to the average ambient temperature of the August month (see Fig. 6), we chose the experimental data on 16th August to validate the modified model in this paper, as shown in Fig. 7. The experimental parameters included the vertical solar radiation, the temperatures of test room, outlet and outside ambient. Comparisons of the simulation with the experiment were illustrated in Figs. 8–11, where 'S' and 'E' mean the simulated and experimental results, respectively.

Figs. 8–11 showed the temperatures of outlet, venetian blinds and massive wall variations with time, respectively. All of the figures indicated that there is good agreement between simulated results and experimental data collected on the test room with the ventilated VBTW. To analyze the error between the simulation and experiment, the root mean square error (RMSE) and mean absolute

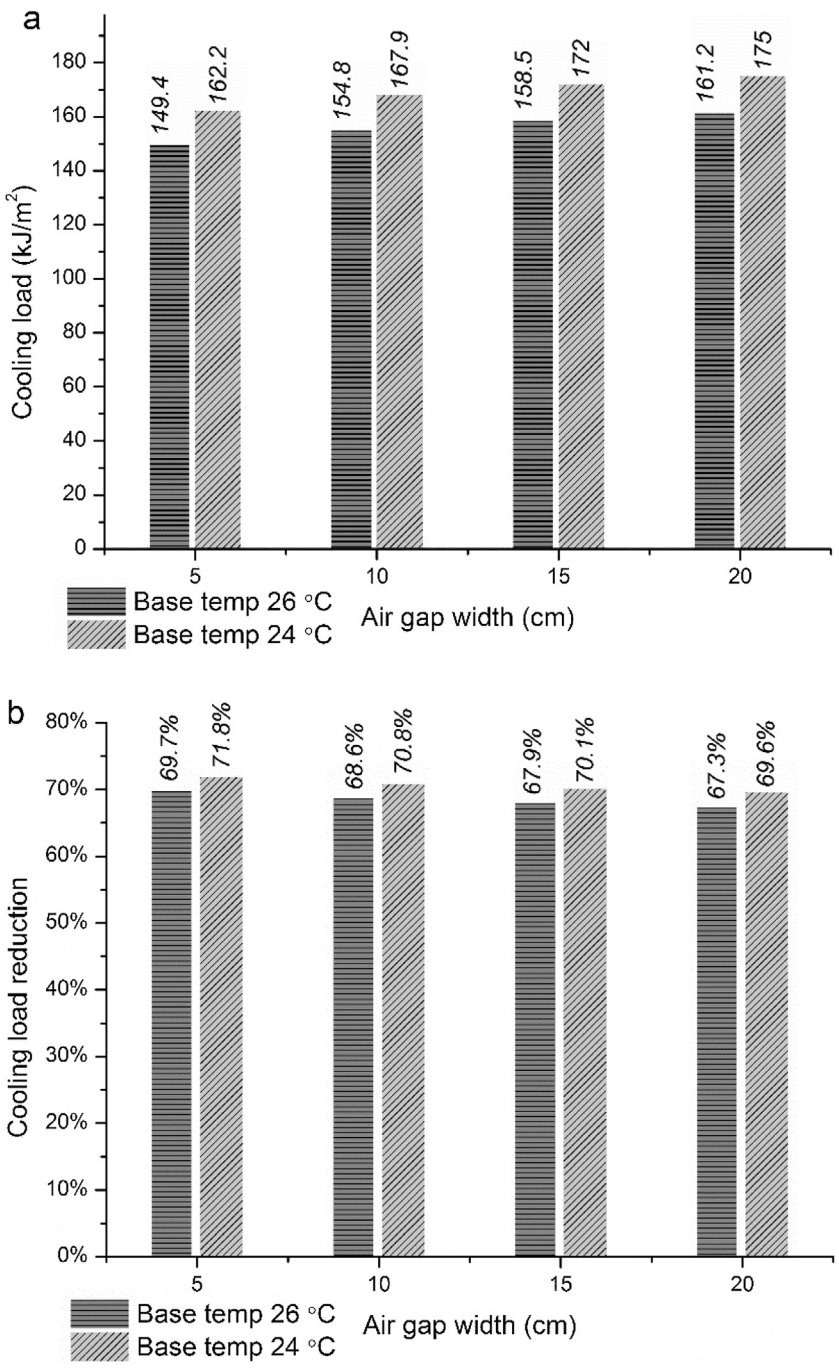

Fig. 12. The effect of air gap width on (a) daily cooling load through the massive wall for 24 °C and 26 °C set-points (b) percentage of cooling load reduction.

error (MAE) are employed in model evaluation. The RMSE and the MAE can be calculated as [27,28]:

$$\mathrm{RMSE} = \sqrt{\frac{1}{n}\sum_{i=1}^{n}(T_{Sim,i} - T_{Exp,i})^2} \tag{33}$$

$$MAE = \frac{1}{n}\sum_{i=1}^{n}|T_{Sim,i} - T_{Exp,i}| \tag{34}$$

where n = 960 in one day in this study (time interval equal to 30 s described in Section 2.2). The corresponding root mean square error (RMSE) and mean absolute error (MAE) were listed in Table 1. The maximum RMSE or MAE did not exceed 0.7 °C. The errors are acceptable from the perspective of a simplified approach. These comparisons demonstrate that the modified model can predict the summer behavior of the ventilated VBTW when used in a building with air conditioner.

4.2. Parametric study

In this section the main results concerning the influence of three parameters on cooling load through the south wall were presented: the blind tilt angles, the air gap width and wall materials in combination with various wall thickness. In addition, two set-point temperatures 24 °C and 26 °C were considered.

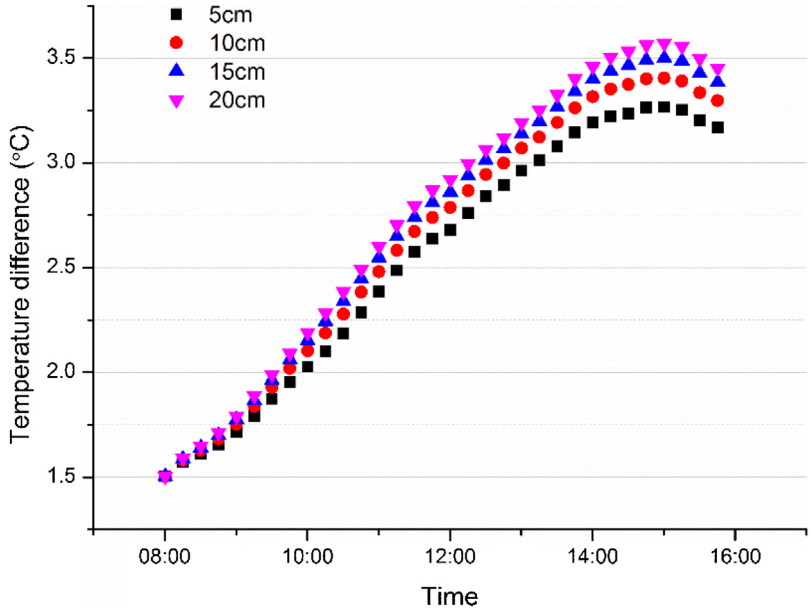

Fig. 13. Temperature difference between the external and internal surface of massive wall for 26 °C set-point.

The ventilation rates ($\dot{V}_{bz}$) of outdoor air supply depend on the occupancy category, which are determined according to ANSI/ASHRAE Standard 62.1-2007 [29]:

$$\dot{V}_{bz} = 3.6 \times (R_p \times P_z + R_a \times A_z) \quad (35)$$

where A_z is the net occupiable floor area of the zone (m^2), P_z is the largest number of people expected to occupy the zone during typical usage, R_p is outdoor airflow rate required per person (L/s person), and R_a is outdoor airflow rate required per unit area (L/s m^2). It is premise of calculating the ventilation rates of outdoor air supply that the floor area is known based on Eq. (35). In this paper, the office space of 20 m^2 was taken as an example. It should be noted that the selection of floor area of an office building was only to determine the volume flow rate of the assisted fan, and the methods used in this paper can be generalized. According to the results listed in Table 2, the minimum ventilation rates of 40 m^3/h was required for an office building of 20 m^2. Therefore, in the following studies the volume flow rate of the assisted fan kept at 40 m^3/h. In addition, it should be mentioned that the glazing and venetian blinds described in Section 2.1 was used in the parametric studies.

4.2.1. Air gap width effect

To investigate the effect of the air gap width on the cooling load, the blind tilt angle and wall properties were considered constant. The massive wall as well as normal south wall was composed of inner lime (10 mm), red brick 1760 (380 mm) and outer lime (10 mm). The blind tilt angle equaled to 80 from the horizontal. The cooling load through the massive wall with various air gap width, 5 cm to 20 cm at 5 cm increment was calculated. The results were shown in Fig. 12a. The percentage of cooling load reduction of the VBTW compared to the normal south wall was also presented in Fig. 12b. As it can be seen by increasing the air gap width, the cooling load was increased a little for 24 °C or 26 °C set-point. For 26 °C set point and 5 cm–20 cm the cooling load reduction was 69.7%–67.3%. For 24 °C set point it was 71.8%–69.6%. Overall, changing the air gap width has no significant effect on the reduction of the cooling load. It was also proved in Fig. 13 that the change of air gap width rarely influenced the temperature difference between the external and internal surface of massive wall for 26 °C set-point. The results were the complement of Ref. [22]. by the present authors. In addition, we found that the effect of air gap width on the heating/cooling performance for the VBTW was similar to other types of Trombe wall, such as classic Trombe wall [30], PV Trombe wall [31].

4.2.2. Blind tilt angle effect

The total solar irradiation transmitted to massive all and airflow inside the air gap were affected by the changes in blind tilt angle. Similar studies on the Double skin façade (DSF) have been conducted by other scholars [32–34] and typically inner and outer layers are glazing structures. However, there is little information about the impacts of the blind tilt angle on the Trombe wall, where internal skin have consisted of material with high thermal mass (massive wall). In this section, the blind tilt angle from the horizontal varied from 15° to 75° in 15° steps intervals, where 75° and 15° relates to almost fully closed and almost fully opened respectively. Based on the above analysis on air gap width, the air gap width of 5 cm was assumed. In addition, the wall materials of red brick 1760 was employed. The energy performance of the VBTW as a result of varying the blind tilt angle was presented in Fig. 14. The results indicated that as the blind tilt angle increases (opening), cooling load through the massive wall increased rapidly. The cooling load reduction of the VBTW compared to the normal south wall was around 10.2% for 24 °C set point and blind tilt angle of 15°. However, it reached up to 70.7% for blind tilt angle of 75°. Therefore, the blind tilt angle with 75° was optimum, i.e. bigger blind tilt angle (closing) yielded lower heat flux across the VBTW. In addition, it should be noted that in the case of 26 °C set point the cooling load became higher after using the VBTW with the blind angle of 15° (see Fig. 14b). Using the VBTW with smaller than 15°during cooling season was strongly not recommended.

4.2.3. Wall material and thickness effect

The aim of this section was to determine the influence of adding a VBTW to different office building envelope constructed with different core layer (see Fig. 4) including materials and thickness. The core layer would be either of concrete or of red brick. The studied core layers were with different densities: two types of red brick, one type of concrete blocks, and one type of concrete. Table 3 showed thermal conductivity, density, and specific heat for different studied core layers. The studied thickness of wall core layer were varied

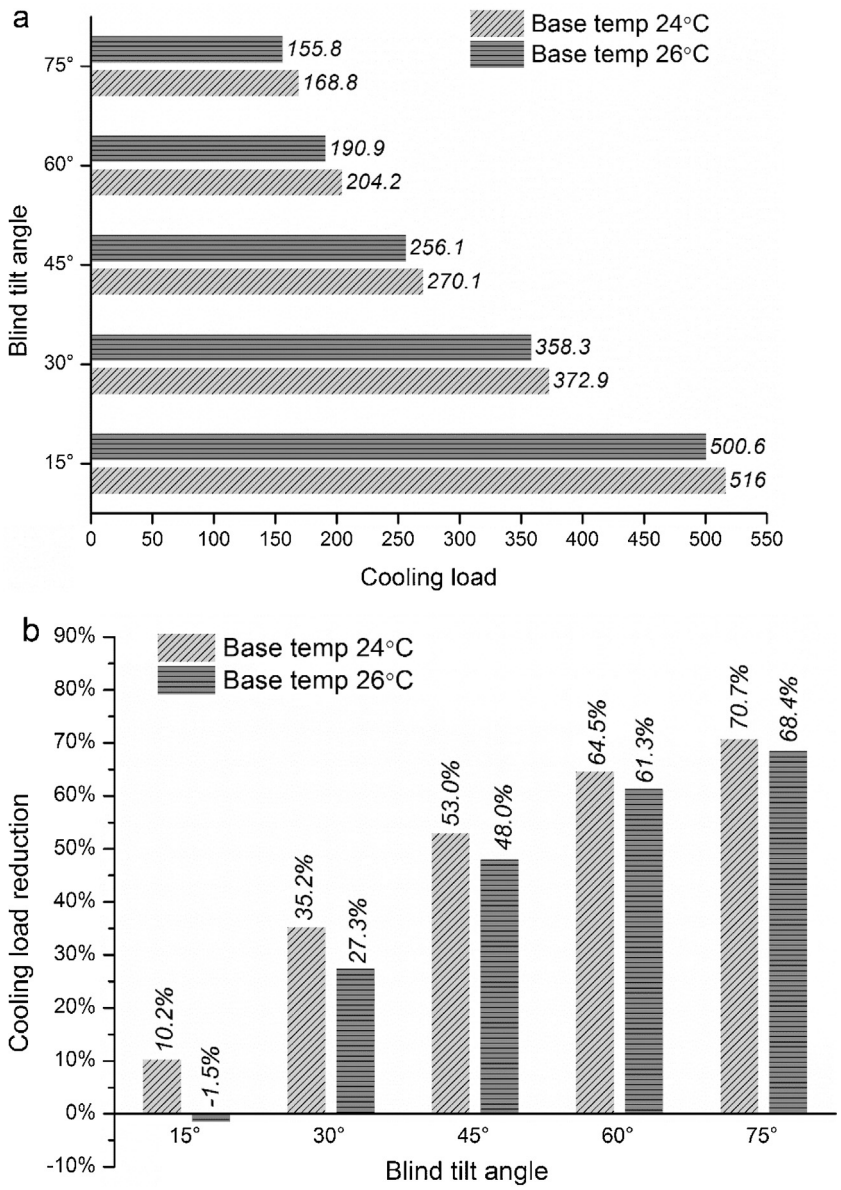

Fig. 14. The effect of blind tilt angle on (a) daily cooling load through the massive wall for 24 °C and 26 °C set-points (b) percentage of cooling load reduction.

Table 3
Properties of the core material used in massive wall as well as normal south wall [35].

Materials	Thermal conductivity (W/m K^{-1})	Density (kg/m^3)	Specific heat (J/kg K^{-1})
Red brick 1120	0.405	1120	840
Red brick 1760	0.78	1760	840
Concrete block 1440	0.33	1440	880
Concrete 2210	1.13	2210	920

180 mm, 280 mm, 380 mm, and 480 mm respectively. At the same time the blind tilt angle of 75° and air gap width of 5 cm were used to find the wall materials effect based on the obtained results. Fig. 15 showed the effect of wall material in combination with various wall thickness on the cooling load through normal wall and massive wall for set-point temperatures 26 °C. The cooling load decreased with the increase of wall core thickness for the same wall material. For the given wall core thickness the use of low instead of high density red brick as well as concrete in the core may reduce the cooling load. This may be explained by the fact that these materials differ in the thermal conductivity. The thermal conductivity of the red brick as well as concrete with higher density was higher. Finally, from Fig. 15 it can been seen that for the same thickness, the cooling load when using the concrete 2210 as core material was biggest, followed by red brick 1760, red brick 1120 and concrete block 1440, in that order. However, the percentage of cooling load reduction was largest for the core material of concrete 2210, as shown in Fig. 16. In addition, it was also observed that the cooling load reduction was nearly same for the use of concrete block 1440 as core material instead of red brick 1120. The obtained results were important in the design phase and few literatures [35] have given the detail investigations on Trombe wall.

The symmetrical surface temperature of the massive wall using the red brick 1120 as core material were presented in Fig. 17, where

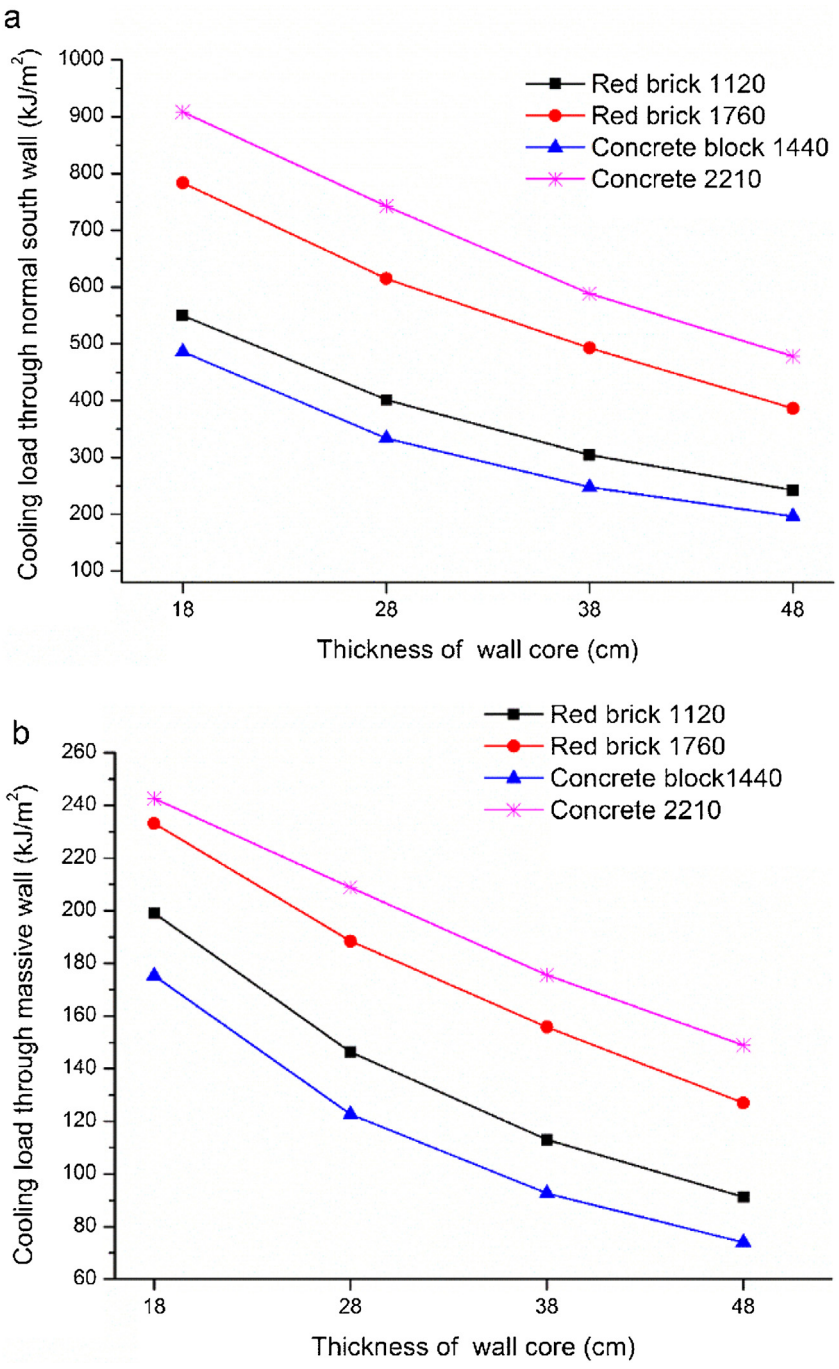

Fig. 15. Cooling load as a function of thickness of wall core layer for different core layer material.

'red brick 1120_180' means the use of 180-mm-thick red brick 1120 as core material. By observing Fig. 17, the rising rate of massive wall temperature decreased with the increase of thickness of wall core layer, resulting in the time lag of heat transfer and more comfortable indoor environment. The findings were in agreement with other research work, revealing that the increase of massive wall's thickness can dampen the wide range heat charge and discharge fluctuation from outdoor [9,11]. By seting thickness of wall core layer at 380 mm, the effect of core material on the symmetrical surface temperature of the massive wall were presented in Fig. 18. It can be seen that the risinging rate of the wall temperature can be arranged in a descending order as follows: red brick 1120 > red brick 1760 > concrete 2210 > concrete block 1440. This depended on the compared thermal conductivity and their thermal capacity.

5. Conclusion

To study the summer behavior of the ventilated VBTW when applied in an office building equipped with a split-type air conditioner, filed measurements were performed in a building located at University of Science and Technology of China, Hefei. Furthermore, a dynamic numerical summer model of the VBTW was developed and validated by the experimental results. Then based on the dynamic model a parametric study was performed to analyze the influence of three parameters on the cooling performance of the ventilated VBTW: the bind tilt angle, air gap width and wall material together with its thickness. In addition, two set-point temperatures 24 °C and 26 °C were considered.

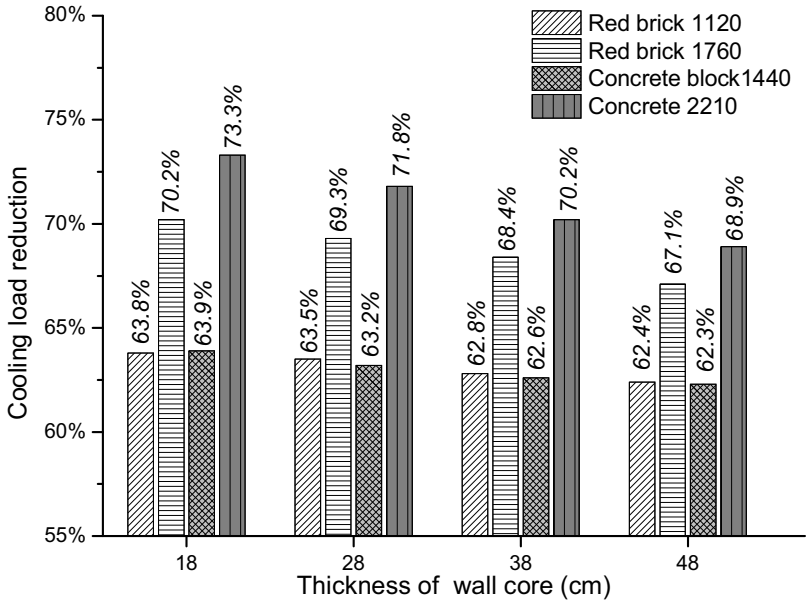

Fig. 16. The percentage of cooling load reduction as a function of thickness of wall core layer.

The air gap width were varied from 5 cm to 20 cm at 5 cm increment. The numerical results indicated that by increasing the air gap width, the cooling load was increased a little for 24 °C or 26 °C set-point. By observing the temperature difference between the external and internal surface of massive wall for 26 °C set-point, it found that air gap width was not significantly effective on the temperature difference. For the given air gap width, changing the blind tilt angle has a significant effect on the cooling load through massive wall. The results indicated that bigger blind tilt angle (closing) yielded lower heat flux across the VBTW. The cooling load reduction of the VBTW compared to the normal south wall was around 10.2% for 24 °C set point and blind tilt angle of 15°. However, it reached up to 70.7% for blind tilt angle of 75°. In addition, it should be noted that in the case of 26 °C set point the cooling load became higher after using the VBTW with the blind angle of 15°. Finally, for set-point temperatures 26 °C the change in wall core materials and thickness indicated that the use of low instead of high density red brick as well as concrete in the core may reduce the cooling load. Besides, the percentage of cooling load reduction was larger for the core material of higher thermal conductivity. With regard to the rate of heat conduct through the massive wall, it depended on the compared thermal conductivity and their thermal capacity.

The afore-mentioned findings are helpful for the energy saving design of the solar utilization. For future studies onsite measurements for a whole year is needed to have an accurate assessment of its efficiency. In addition, a post-occupancy evaluation should be conducted to measure occupants' satisfaction and whether it fulfills their perceptions of comfort. The cost efficiency and the payback time of the proposed system should be also analyzed as it is important before introducing it to the local market.

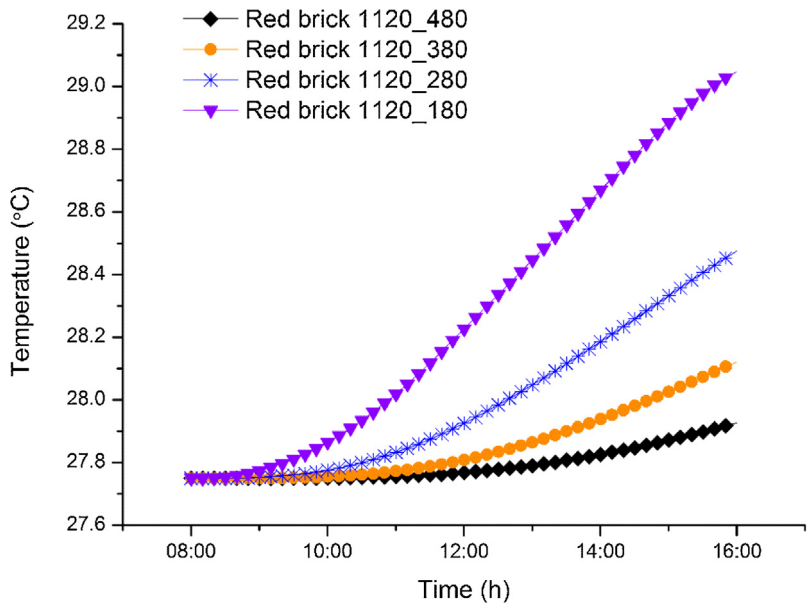

Fig. 17. Symmetrical surface temperature of the massive wall (see Fig. 4) as a function of thickness of wall core layer for red brick 1120.

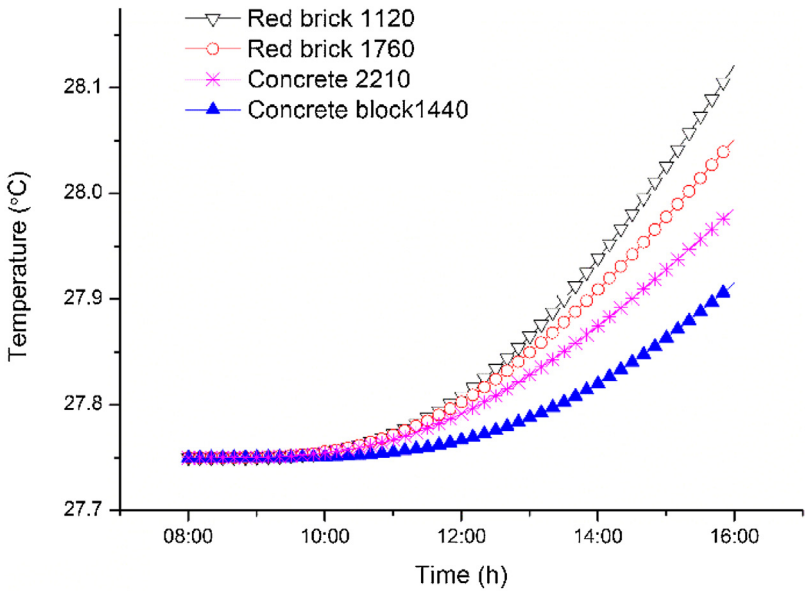

Fig. 18. Symmetrical surface temperature of the massive wall (see Fig. 4) as a function of wall core material for 380-mm-thick core layer.

Acknowledgments

This research was supported by the grants from the Twelfth Five-Year Science and Technology Support Key Project of China (No. 2012BAJ08B04), Program for New Century Excellent Talents in University (No. NCET-11-0876) and also Dongguan innovative research team program (No. 2014607101008).

References

[1] M. Ghalamchi, A. Kasaeian, M. Ghalamchi, Experimental study of geometrical and climate effects on the performance of a small solar chimney, Renew. Sust. Energy Rev. 43 (0) (2015) 425–431.
[2] S. Jaber, S. Ajib, Optimum design of Trombe wall system in mediterranean region, Sol. Energy 85 (9) (2011) 1891–1898.
[3] J. Hirunlabh, W. Kongduang, P. Namprakai, J. Khedari, Study of natural ventilation of houses by a metallic solar wall under tropical climate, Renew. Energy 18 (1) (1999) 109–119.
[4] J. Kachadorian, The Passive Solar House: The Complete Guide to Heating and Cooling Your Home, Chelsea Green Publishing Company, 2006.
[5] H.-Y. Chan, S.B. Riffat, J. Zhu, Review of passive solar heating and cooling technologies, Renew. Sustain. Energy Rev. 14 (2) (2010) 781–789.
[6] L. Zalewski, S. Lassue, B. Duthoit, M. Butez, Study of solar walls—validating a simulation model, Build. Environ. (2002).
[7] M.F. Hordeski, Dictionary of Energy Efficiency Technologies, The Fairmont Press, Inc., 2004.
[8] A.J.N. Khalifa, E.F. Abbas, A comparative performance study of some thermal storage materials used for solar space heating, Energy Build. 41 (4) (2009) 407–415.
[9] A. Briga-Sá, A. Martins, J. Boaventura-Cunha, J.C. Lanzinha, A. Paiva, Energy performance of Trombe walls: adaptation of ISO 13790:2008(E) to the Portuguese reality, Energy Build. 74 (2014) 111–119.
[10] V.C. Nelson, Introduction to Renewable Energy, CRC press, 2011.
[11] C. Bin, C. Cuiying, Y. Wenxiu, A calculation model of passive solar house with Trombe wall, Renew. Energy Proc. (2006).
[12] B. Agrawal, G.N. Tiwari, Building integrated photovoltaic thermal systems: for sustainable developments, R. Soc. Chem. (2011).
[13] B. Chen, X. Chen, Y.H. Ding, X. Jia, Shading effects on the winter thermal performance of the Trombe wall air gap: an experimental study in Dalian, Renew. Energ. 31 (12) (2006) 1961–1971.
[14] N. Ghrab-Morcos, C. Bouden, R. Franchisseur, Overheating caused by passive solar elements in Tunis: effectiveness of some ways to prevent it, Renew. Energ. 3 (6) (1993) 801–811.
[15] J. Ji, H. Yi, W. He, G. Pei, PV-Trombe wall design for buildings in composite climates, J. Solar Energy Eng. 129 (4) (2007) 431.
[16] M. Soussi, M. Balghouthi, A. Guizani, Energy performance analysis of a solar-cooled building in Tunisia: passive strategies impact and improvement techniques, Energy Build. 67 (2013) 374–386.
[17] G. Gan, Simulation of buoyancy-induced flow in open cavities for natural ventilation, Energy Build. 38 (5) (2006) 410–420.
[18] G. Gan, A parametric study of Trombe walls for passive cooling of buildings, Energy Build. 27 (1) (1998) 37–43.
[19] F. Stazi, A. Mastrucci, C. di Perna, Trombe wall management in summer conditions: an experimental study, Sol. Energy 86 (9) (2012) 2839–2851.
[20] M. Rabani, V. Kalantar, A.A. Dehghan, A.K. Faghih, Empirical investigation of the cooling performance of a new designed Trombe wall in combination with solar chimney and water spraying system, Energy Build. 102 (2015) 45–57.
[21] M. Rabani, V. Kalantar, A.A. Dehghan, A.K. Faghih, Experimental study of the heating performance of a Trombe wall with a new design, Sol. Energy 118 (2015) 359–374.
[22] X. Hong, W. He, Z. Hu, C. Wang, J. Ji, Three-dimensional simulation on the thermal performance of a novel Trombe wall with venetian blind structure, Energy Build. 89 (2015) 32–38.
[23] W. He, Z. Hu, B. Luo, X. Hong, W. Sun, J. Ji, The thermal behavior of Trombe wall system with venetian blind: an experimental and numerical study, Energy Build. 104 (2015) 395–404.
[24] H.B. Awbi, Ventilation of Buildings, Taylor & Francis, 2003.
[25] A. Bejan, Convection Heat Transfer, John wiley & sons, 2013.
[26] W. Sun, J. Ji, C. Luo, W. He, Performance of PV-Trombe wall in winter correlated with south façade design, Appl. Energ. 88 (1) (2011) 224–231.
[27] C.J. Willmott, K. Matsuura, Advantages of the mean absolute error (MAE) over the root mean square error (RMSE) in assessing average model performance, Clim. Res. 30 (1) (2005) 79.
[28] T. Chai, R.R. Draxler, Root mean square error (RMSE) or mean absolute error (MAE)?–Arguments against avoiding RMSE in the literature, Geosci. Model Dev. 7 (3) (2014) 1247–1250.
[29] A. Ashrae, Standard 62. 1-007, ventilation for acceptable indoor air quality, in: American Society of Heating, Air-Conditioning and Refrigeration Engineers, in, Inc., 2007.
[30] Z. Yilmaz, A. Basak Kundakci, An approach for energy conscious renovation of residential buildings in Istanbul by Trombe wall system, Build. Environ. 43 (4) (2008) 508–517.
[31] J. Peng, L. Lu, H. Yang, J. Han, Investigation on the annual thermal performance of a photovoltaic wall mounted on a multi-layer façade, Appl. Energy 112 (2013) 646–656.
[32] D. Iyi, R. Hasan, R. Penlington, C. Underwood, Double skin façade: modelling technique and influence of venetian blinds on the airflow and heat transfer, Appl. Therm. Eng. 71 (1) (2014) 219–229.
[33] T.E. Jiru, Y.-X. Tao, F. Haghighat, Airflow and heat transfer in double skin facades, Energy Build. 43 (10) (2011) 2760–2766.
[34] N. Safer, M. Woloszyn, J.J. Roux, Three-dimensional simulation with a CFD tool of the airflow phenomena in single floor double-skin facade equipped with a venetian blind, Sol. Energy 79 (2) (2005) 193–203.
[35] M. Bojić, K. Johannes, F. Kuznik, Optimizing energy and environmental performance of passive Trombe wall, Energy Build. 70 (2014) 279–286.